Tissue classification for laparoscopic image understanding based on multispectral texture analysis

Yan Zhang[a], Sebastian J. Wirkert[a], Justin Iszatt[a], Hannes Kenngott[b], Martin Wagner[b], Benjamin Mayer[b], Christian Stock[c], Neil T. Clancy[d,e], Daniel S. Elson[d,e] and Lena Maier-Hein[a]

[a]Computer-Assisted Interventions, German Cancer Research Center, Heidelberg, Germany;
[b]Department for General, Visceral and Transplantation Surgery, Heidelberg University Hospital, Heidelberg, Germany;
[c]Institute of Medical Biometry and Informatics, University of Heidelberg, Heidelberg, Germany;
[d]Hamlyn Centre for Robotic Surgery, Institute of Global Health Innovation, Imperial College London, London, UK;
[e]Department of Surgery and Cancer, Imperial College London, London, UK

ABSTRACT

Intra-operative tissue classification is one of the prerequisites for providing context-aware visualization in computer-assisted minimally invasive surgeries. As many anatomical structures are difficult to differentiate in conventional RGB medical images, we propose a classification method based on multispectral image patches. In a comprehensive *ex vivo* study we show (1) that multispectral imaging data is superior to RGB data for organ tissue classification when used in conjunction with widely applied feature descriptors and (2) that combining the tissue texture with the reflectance spectrum improves the classification performance. Multispectral tissue analysis could thus evolve as a key enabling technique in computer-assisted laparoscopy.

Keywords: tissue classification, multispectral laparoscopy, multispectral texture analysis

1. INTRODUCTION

In contrast to traditional open surgery, laparoscopy is less invasive, causing smaller incisions and providing shorter recovery periods. One recent direction of research focuses on offering context-aware guidance (e.g. warning signals emitted when sharp instruments approach structures at risk) where computer assistance is provided, depending on the current phase within the medical procedure. Situation recognition from sensor data, however, is extremely challenging and requires a good understanding of the scene. In this context, the classification of tissue may provide important cues with respect to what is currently happening.

In recent years, several methods for tissue or organ classification have already been proposed (e.g.[1,2]), which are based on gray-value or RGB images. More recently, multispectral (or hyperspectral) imaging techniques have achieved success in cancer detection and tissue classification.[3] Multispectral images generally have tens or hundreds of channels, each of which corresponds to the reflection of light within a certain wavelength band. Therefore they can provide high spectral resolution and reveal optical tissue characteristics. Multispectral tissue classification methods as mentioned in the literature so far mainly use the image pixel, which corresponds to a reflectance spectrum at a specific position, as their feature descriptor.[4,5] Given the recent success of multispectral texture analysis outside of the field of laparoscopy,[6,7] the hypothesis proposed by this paper is that texture-based methods can improve multispectral organ classification.

To our knowledge we are the first to address the problem of tissue classification based on multispectral texture analysis for intra-operative laparoscopy. The contribution of this paper is two-fold: (1) We investigate organ tissue classification in a laparoscopic setup and perform a comprehensive *ex-vivo* study, showing that multispectral images are superior to RGB images for tissue classification in laparoscopy. (2) We propose a feature descriptor combining texture and spectral information based on only a small number of specified bands.

Medical Imaging 2016: Image-Guided Procedures, Robotic Interventions, and Modeling,
edited by Robert J. Webster III, Ziv R. Yaniv, Proc. of SPIE Vol. 9786, 978619
 · doi: 10.1117/12.2216090

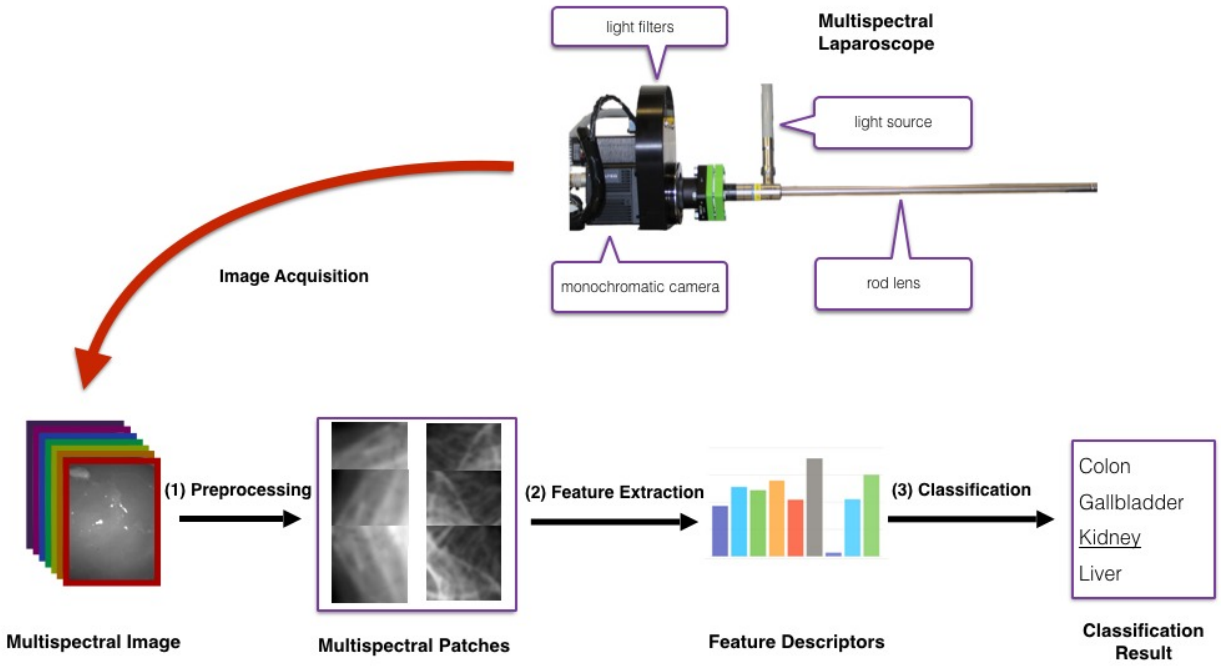

Figure 1. Concept for multispectral tissue classification. After multispectral image acquisition, noise is removed and the resulting image is cropped into patches (1). From each of these patches the local binary pattern texture feature and the average spectrum are calculated (2) and fed into a support vector machine model to classify the organ characterized by the patch under investigation (3).

2. MATERIALS AND METHODS

This section encompasses three central parts of our work: the multispectral image acquisition using a custom-built laparoscope (Sect. 2.1), feature extraction, classification (Sect. 2.2) and description of the experiments in Sect. 2.3. An overview of the proposed approach is visualized in Fig. 1.

2.1 Hardware

Multispectral images are captured using a custom-built multispectral laparoscope, which is shown in Figure 1. It combines a Richard Wolf (Knittlingen, Germany) laparoscope and light source with the 5Mpixel Pixelteq Spectrocam (Largo, FL, USA). Following the recommendation by Wirkert et al.,[8] we use light filters with central wavelengths of $470nm$, $480nm$, $511nm$, $560nm$, $580nm$, $600nm$, $660nm$ and $700nm$. The full width at half maximum (FWHM) of the bands is 20nm, except for the 480nm band where it is 25nm. The camera runs at $20fps$.

As the camera does not provide RGB images directly, we select the channels of $470nm$, $560nm$ and $700nm$ and regard them as blue, green and red. Note that our synthetic RGB image contains more specific information than a true RGB image, as it is composed of bands with a Full Width Half Maximum of $20nm$, thus being much narrower than true RGB bands.

2.2 Tissue Classification

Given the captured images, the workflow consists of three steps: (1) preprocessing, (2) feature extraction and (3) classification. Each step is described in the following paragraphs.

2.2.1 Preprocessing

Image preprocessing converts multispectral raw images into multispectral patches, involving noise removal and patch extraction. Since Gaussian noise usually exists in the raw image, we apply Total Variation[9] in this paper, which is able to remove Gaussian noise while preserving sharp edges. Afterwards, we select several rectangular patches from the multispectral images. These patches all have the same size.

2.2.2 Feature Extraction

In the feature extraction step, a feature vector is extracted from the spatial neighborhood and spectral profile of each pixel, serving as a (multispectral) fingerprint to enable tissue classification. The pixels' local context can be represented by texture, since one specific type of tissue usually possesses characteristic repeating patterns on the surface; the optical characteristics, comprising absorption and scattering properties, are influencing the pixels' spectral profile.[10] As laparoscopic images are captured from various viewpoints under various illumination conditions, the extracted features should be robust to the pose of the endoscope as well as to the lighting conditions. Furthermore, they should be computationally cheap in order to enable real-time image processing in future applications. Numerous texture descriptors have been proposed in the literature[11] but only few of them are suitable for our purposes. In this paper, we use the local binary pattern[12] to extract texture information; we also use the averaged spectrum to extract spectral information.

Local Binary Pattern (LBP). Local Binary Pattern[12] is a robust texture representation method, which encodes local primitive micro-structures in the image. It is already being successfully used for other purposes such as face detection.[13,14] In a 2D gray-scale image $I(\mathbf{x})$, a circle with radius R is centered at every pixel, and P points on the circle are compared with the center pixel. One can then extract a binary string at every location within the image and obtain a local binary pattern map $LBP_{P,R}$, which can be formulated as

$$LBP_{P,R}(\mathbf{x}) = \sum_{p=0}^{P-1} \delta(I(\mathbf{x}_p) - I(\mathbf{x})) \cdot 2^p \tag{1}$$

with

$$\delta(s) = \begin{cases} 1, s \geq 0 \\ 0, \text{otherwise} \end{cases}, \tag{2}$$

where $\mathbf{x}_p$ is the point on the circle, the gray-value of which is computed via interpolation. The occurrence histogram of the **LBP** map is regarded as the feature descriptor.

LBP is gray-scale invariant and provides low computational complexity, which is beneficial to the implementation of real-time uses. The study of Ojala et al.[12] proposes an advanced version named $\mathbf{LBP}^{riu2}_{P,R}$, which provides rotational invariance and only contains uniform patterns for representative microstructures. One can refer to the study of O. Lahdenoja et al.[15] for more insights. We extract patterns with three (P, R) combinations for multiple resolutions[12] and repeat this computation at each image channel in order to capture texture information at every spectral band. To improve the robustness, we normalize the feature vector from each occurrence histogram. In this paper, we use the name **LBP** to denote our local binary pattern presented herein, which is uniform and rotationally invariant while offering multiresolution analysis.

Average Spectrum (AS). Spectral reflectances of one location within a multispectral image could directly be extracted and used as the feature descriptor. Such a type of spectral feature descriptor would offer a high spatial resolution. However, it would be only feasible if all bands were already precisely aligned and if no noise existed.

We average all the spectral reflectances around one location in each channel, sacrificing high spatial resolution but improving the robustness against noise. Given one location $\mathbf{x}$ within a multispectral image I, the spectral feature vector $\boldsymbol{\phi}$ is given by

$$\phi_c = \frac{1}{|\mathcal{N}|} \cdot \sum_{\mathbf{y} \in \mathcal{N}(\mathbf{x})} I_c(\mathbf{y}) \ , \tag{3}$$

where $\mathcal{N}(\mathbf{x})$ is the neighbor set of $\mathbf{x}$ and c is the band index. One can find a similar feature descriptor in the literature.[5] Since multispectral image patches are used in this paper, we set the point $\mathbf{x}$ at the center of the patch with the neighbor set $\mathcal{N}$ containing all remaining locations. To compensate for scaling in cases where the illumination condition changes, we normalize the feature vector to the unit length.

AS+LBP. Since the texture information mainly represents spatial characteristics in each band and the spectral information mainly represents underlying optical properties, we hypothesize that **AS** and **LBP** represent complementary information. We therefore propose the combined feature descriptor **AS+LBP**, which is a concatenation of the two feature vectors.

2.2.3 Classification

In this paper, we apply a support vector machine (SVM) model with a Gaussian kernel to discriminate tissues. Due to its advantages mentioned in the literature,[16] it is suitable to address the classification problem in our scenario. Firstly, it overcomes *curse-of-dimensionality*. Since high-dimensional data as ours is explicitly handled by the kernel function, parameter proliferation is prevented in the high-dimensional feature space, leading to trackable computation and limited over-fitting. Secondly, derived from the statistical learning theory, the SVM model can provide complex decision functions and therefore can fit the data well. Thirdly, the SVM solution is only determined by the support vectors, so that its performance is potentially repeatable when the training data has small disturbances.

Given a set of training data $\{(\boldsymbol{x}_i, y_i)\}_{i=1}^n$ with $y_i \in \{1, -1\}$, the SVM model can be given by its dual formula[17]

$$\begin{aligned} \boldsymbol{\alpha}^* = &\max_{\alpha_i} \left\{ \sum_{i=1}^n \alpha_i - \frac{1}{2} \sum_{i,j=1}^n \alpha_i \alpha_j y_i y_j k(\boldsymbol{x}_i, \boldsymbol{x}_j) \right\} \\ \text{subject to } &0 \le \alpha_i \le \frac{C}{n}, \forall i = 1, 2, ..., n \\ &\sum_{i=1}^n \alpha_i y_i = 0 \end{aligned} \tag{4}$$

and the decision function f can be given by

$$f(\boldsymbol{x}) = \operatorname{sgn} \left(\sum_{i=1}^n \alpha_i^* y_i k(\boldsymbol{x}, \boldsymbol{x}_i) + b \right) \ , \tag{5}$$

where the threshold b can be computed by an averaging procedure, the kernel function $k(\mathbf{x}, \mathbf{y}) = e^{-\gamma \cdot |\mathbf{x}-\mathbf{y}|^2}$ and C is the hyper-parameter governing the regularization weight.

The Gaussian kernel-based SVM only have two hyper-parameters, i.e. the Gaussian kernel size γ and the regularization weight C, to specify and usually achieves satisfactory performances in practice. To perform multi-class classification, we use a *one-against-one* scheme for SVM in this paper and optimize the two model hyper-parameters via grid search and cross validation. Since SVM is sensitive to the data scale, we normalize the feature vector of each sample to the unit length and perform standardization within each feature dimension.

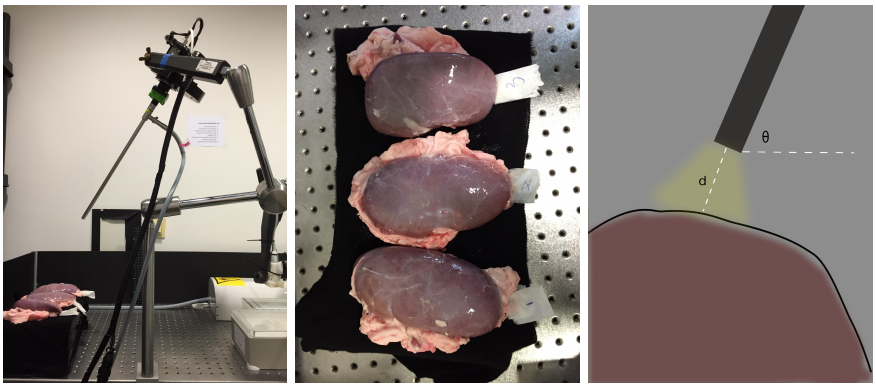

Figure 2. Setup for capturing multispectral images of kidney tissue. **From left to right:** The multispectral laparoscope. The three porcine kidneys originating from three different pigs. Camera pose, where the red region denotes the tissue and the black bar denotes the rod lens. Additionally, the yellow region denotes the light and the dark background indicates that images are captured in a dark environment.

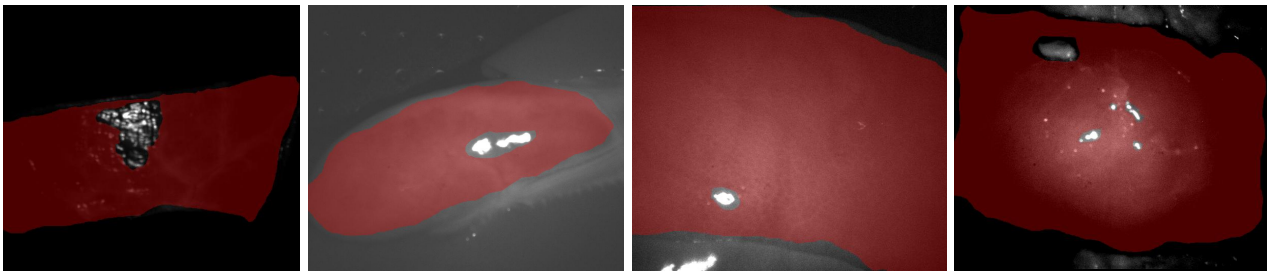

Figure 3. Image annotation is completed by excluding areas not covered by tissue and exposure regions. The regions to classify are annotated by in red. **From left to right:** Colon, gallbladder, liver and kidney.

2.3 Experiments

The goal of our experiments was to verify the superiority of the multispectral image compared to the RGB image and the benefits of combining texture information and spectral information in organ tissue classification. For these purposes, we discriminated in our experiment four types of porcine organ tissues typically encountered during hepatic laparoscopic surgeries: liver, gallbladder, colon and kidney, which have been collected from three different pigs. The laparoscopic setup is illustrated by Figure 2, which shows the process of capturing multispectral images of kidney tissue. When capturing images, the light was only provided by the laparoscopic light source. We targeted the rod lens to a smooth region of each organ whose mean surface normal was approximately perpendicular to the horizontal plane and captured images by varying the camera pose. The camera pose is defined by (θ, d), where θ is the angle between the the rod lens and the horizontal plane and d is the distance between the lens tip and the organ surface. We specify $(\theta, d) \in \{30\,^\circ, 60\,^\circ, 90\,^\circ\} \times \{4cm, 5.5cm, 7cm\}$, as these distances and angles are typically encountered during laparoscopic surgeries.[18] Therefore, we obtained an image set containing 27 subsets for each organ denoted by $(pig_i, \theta_j, d_k) \in \{pig_1, pig_2, pig_3\} \times \{30\,^\circ, 60\,^\circ, 90\,^\circ\} \times \{4cm, 5.5cm, 7cm\}$, in which the images feature diverse anatomical structures and illumination conditions.

After capturing multispectral raw images, we performed the preprocessing procedures mentioned in Section 2.2.1. For the training purpose, we annotated regions in each multispectral image as reference and also marked invalid regions such as exposure caused by specular reflection using MITK.[19] We then assigned a label to the image reference. Some image annotation results are illustrated in Figure 3. Each multispectral image was cropped into several patches of a size 300 × 300 pixels. From these 100 patches were randomly selected, following the criterion that at least 80% of each image patch needed to overlap with the annotated reference. These selected patches were then stored in a multispectral patch set named $\mathcal{S}$, which is illustrated by Figure 4. Consequently, the patch set $\mathcal{S}$ is well balanced.

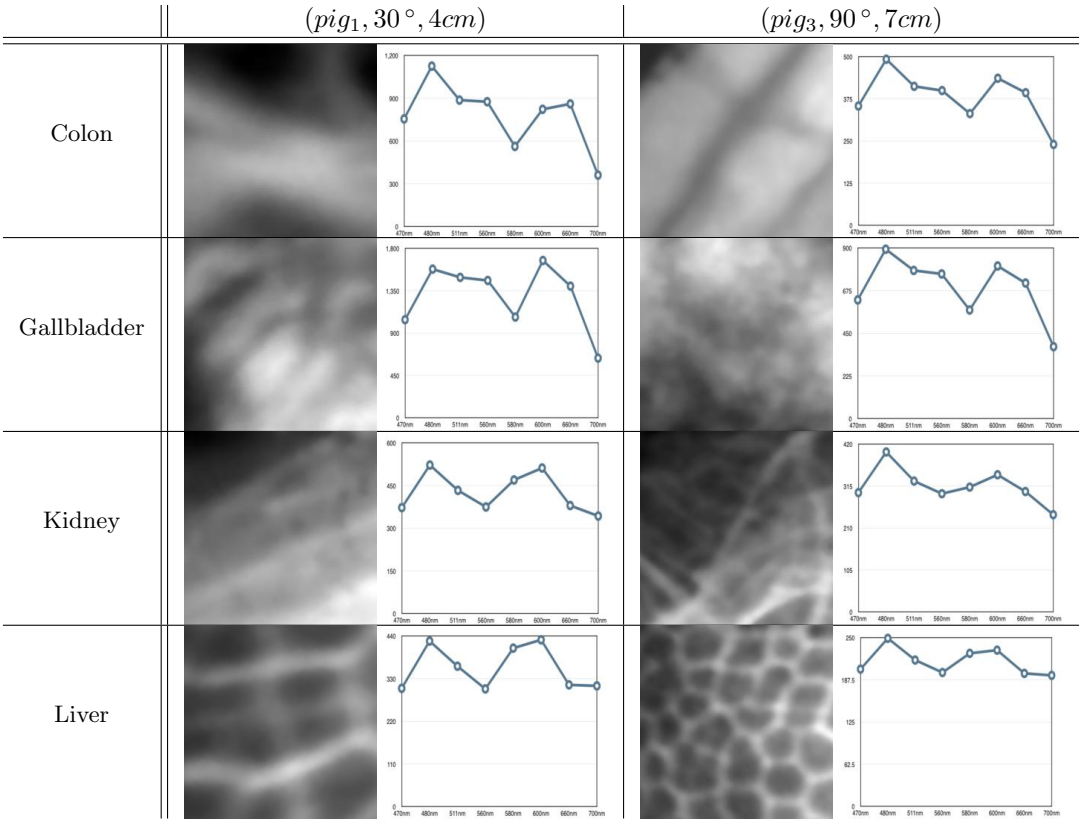

Figure 4. Eight patches from two subsets in $\mathcal{S}$ and the associated averaged spectrum of each patch. The patches have been extracted from the image corresponding to the central wavelength of $470nm$. In each spectrum plot, the x axis denotes the wavelength and the y axis denotes the reflectance.

For each multispectral image patch, we extracted its texture feature **LBP**, its spectral feature **AS** and its combined textural/spectral feature **AS+LBP**. For comparison purposes, we also used two other commonly used feature description methods: the Gabor filter banks (**GFB**) and the gray-level co-occurrence matrix (**GLCM**)[11] *. As with LBP, these methods were applied to each channel and the feature vectors were concatenated.

The classification test was performed on every subset of $\mathcal{S}$ in turn, i.e. when the performance was tested on (pig_i, θ_j, d_k), the classifier is trained on $\{(pig_{i'}, \theta_{j'}, d_{k'}) \mid i' \neq i\}$. To test the influence of camera pose changes, we excluded the camera pose in the testing set from the training set. Specifically, when testing on (pig_i, θ_j, d_k), the classifier was trained on $\{(pig_{i'}, \theta_{j'}, d_{k'}) \mid i' \neq i, j' \neq j, k' \neq k\}$.

During the training phase, the two hyper-parameters C and γ in the SVM model are optimized via grid search and cross validation †. The classification performance is evaluated by the accuracy rate (100%-test error), which is the ratio of correctly classified samples to all samples in the testing set. This evaluation does not give biased results in our scenario since our dataset is balanced.

3. RESULTS

The accuracy rates are shown in terms of box plots in Figure 5. Comparing the two box plots in each row, one can observe that: (1) The performance using the multispectral imaging data is better than the performance using the RGB imaging data for all feature descriptors; (2) when excluding the camera pose used in the testing data from the training data, all performances deteriorate; (3) the proposed feature descriptor **AS+LBP** performs best in each case.

*These three texture representation methods are implemented via the Python module *scikit-image*.

†The SVM classification and hyper-parameter selection are implemented based on the Python library *scikit-learn*.

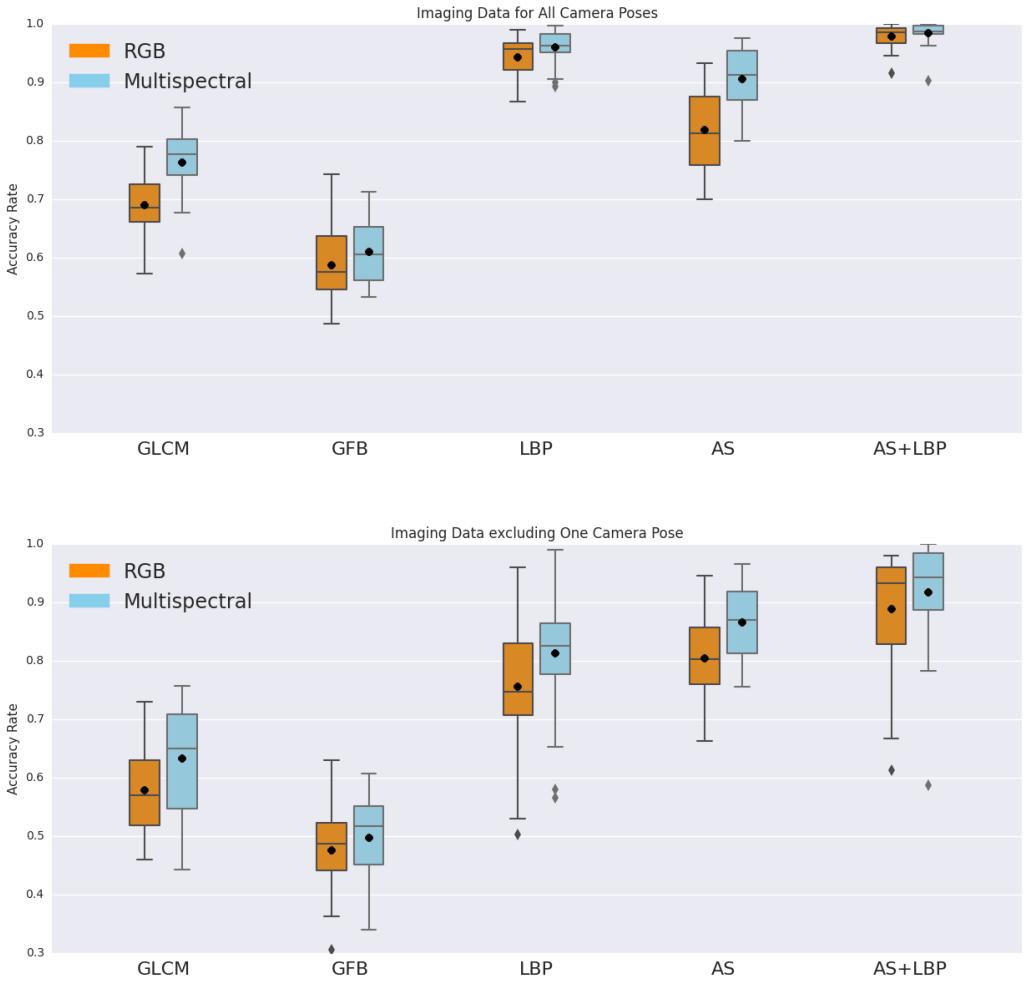

Figure 5. Accuracy obtained for different descriptors using RGB data (orange) and eight channels of multispectral data (blue). Each box extends from the first quartile to the third quartile. The whiskers denote the range from the 5th percentile to the 95th percentile. Outliers are visualized as well. In each figure, the horizontal axis shows the feature description methods. The vertical axis indicates the accuracy rate. The black point and the gray bar within each box denote the mean and the median of accuracy rates respectively. **The first row:** All camera poses are incorporated in the training set. **The second row:** The camera pose used in testing set is excluded from the training set.

In addition, the median accuracy rates given in Table 1 correspond to the gray bars in the boxplots. For each feature, the improvement from the RGB image to the multispectral image is equal to the accuracy rate difference divided by the accuracy rate of RGB data. The median improvement in accuracy obtained by using multispectral data as opposed to RGB data is 7% on average.

One can also see the benefit of combining texture information and spectral information. For multispectral imaging data, the feature **AS+LBP** outperforms **AS** by 8% and **LBP** by 2% when all camera poses are considered. When one camera pose is excluded from training, the feature **AS+LBP** outperforms **AS** by 8% and **LBP** by 14%.

Table 1. Median accuracy rates, which correspond to the gray bars in Figure 5.

	All camera poses are considered.					One camera pose is excluded.				
	GLCM	**GFB**	**LBP**	**AS**	**AS+LBP**	**GLCM**	**GFB**	**LBP**	**AS**	**AS+LBP**
RGB	68.5%	57.5%	95.8%	81.3%	97.8%	57.0%	48.7%	74.8%	80.2%	93.3%
Multispectral	77.7%	60.5%	96.3%	91.2%	98.4%	65.0%	51.7%	82.5%	87.0%	94.3%
Improvement	13.4%	5.2%	0.52%	12.2%	0.61%	14.0%	6.2%	10.3%	8.5%	1.1%

4. DISCUSSION

To our knowledge, we are the first to investigate organ tissue classification in a laparoscopic setup based on multispectral texture analysis. Our method classifies image patches based on both textural (**LBP**) and spectral (**AS**) features. We show in the experiment results, when using equal feature descriptors and classification methods, the multispectral image leads to higher accuracy rates than the RGB image in all but one cases (see Table 1). We therefore conclude that the multispectral image is superior to the RGB image in our scenario. This fact further indicates that the multispectral image contains more information than the RGB image.

To represent texture information, we used **LBP**, which is rotationally invariant, gray-scale invariant and accounts for multiple resolutions. We also investigated **GLCM** and **GFB** texture features as baseline methods. The **GLCM** lacks robustness to illumination and geometry variations in nature, which probably causes its weaker performance in comparison with **LBP**. The **GFB** also performs worse than **LBP**, which could be caused by the non-optimal parameters of the filter bank. According to the literature,[20] the filter bank parameters determining the feature quality are highly dependent on the texture type. In our tissue classification scenario, the texture is diverse from image to image, even from training images to test images. This issue causes parameter selection to be a highly challenging task. From the computational perspective, large memory consumption for **GLCM**[21] and high computational complexity for **GFB**[20] are reported, while **LBP** can be calculated rapidly and has low memory consumption.[12] Thus, we conclude that **LBP** is the best texture descriptor among the three commonly used texture descriptors both from a performance as well as a computational standpoint.

The feature **AS** is proposed to capture spectral information. Due to the averaging operation, **AS** is potentially robust to noise and of low spatial resolution. Due to the applied l2-normalization it is also robust to multiplicative changes in illumination. During computer-assisted surgeries, however, tissues usually deform in a non-rigid manner and real-time image registration in this scenario is highly challenging.[22] Future work should thus investigate whether simple averaging is sufficient for ensuring descriptor robustness in the presence of motion. Furthermore, we extract the feature **AS** from the square image patch at the current stage. We expect that using a circular patch would improve the robustness to rotation.

As shown in the experimental results, the proposed texture-spectral feature **AS+LBP** outperforms other features and also its own individual components, verifying that the texture information complements the spectral information. In our experiments, we captured images from multiple viewpoints with different illumination conditions to simulate challenges encountered during laparoscopic interventions, the classifier however cannot cover all geometrical variations encountered during surgeries. This is verified by the accuracy decreasing when

one camera pose is excluded from the training data, as shown in Figure 5 and Table 1. The results also suggests that complicated geometric variations can, and should, be learned.

We performed a comprehensive *ex vivo* study on organ tissue classification to provide a basis for tissue classification in the clinical intraoperative scenario. However, our study has some limitations. Firstly, compared to the *ex vivo* experiment, *in vivo* laparoscopic interventions cause new challenges, such as organ deformation during image capturing, internal bleeding and optical characteristic shifting due to tissue perfusion. To address these challenges we aim to collect more data using an *in vivo* setting and to create a benchmark for multispectral organ classification in laparoscopy.
Secondly, although we have chosen efficient textural and spectral descriptors, an in-depth run-time analysis to investigate the real-time capabilities of the proposed approach has not yet been performed. These were not the focus of this study, which used Python implementation of the algorithms. The run-time analysis will be made after the approach has been ported to real clinical uses, for which we expect the implementation to be optimized using an efficient programming language.
Thirdly, it would be interesting to investigate different classifiers, such as Random Forests and deep neural networks, especially when the amount of data is large. Additionally, if *in vivo* and *ex vivo* data are combined, the covariance shift due to the translation to perfused tissue could be combated by applying domain adaptation methods.[23]

Conclusion. This paper provides a comprehensive study of organ tissue classification based on multispectral texture analysis. According to our experiments, we show that, compared with the RGB image, the multispectral image is superior for tissue classification. Based on a multispectral image with eight bands, the novel feature descriptor combining texture and spectral information achieves highly accurate classification results. Therefore, we suggest that using multispectral imaging data is beneficial for organ tissue classification in laparoscopy.

Acknowledgement Funding for this work was provided by the European Research Council (ERC) starting grant COMBIOSCOPY (637960).

REFERENCES

[1] Lee, J., Oh, J., Shah, S. K., Yuan, X., and Tang, S. J., "Automatic classification of digestive organs in wireless capsule endoscopy videos," in [*Proceedings of the 2007 ACM symposium on Applied computing*], 1041–1045, ACM (2007).

[2] Azzopardi, C., Hicks, Y. A., and Camilleri, K. P., "Exploiting gastrointestinal anatomy for organ classification in capsule endoscopy using locality preserving projections," in [*Engineering in Medicine and Biology Society (EMBC), 2013 35th Annual International Conference of the IEEE*], 3654–3657, IEEE (2013).

[3] Lu, G. and Fei, B., "Medical hyperspectral imaging: a review," *Journal of biomedical optics* **19**(1), 010901–010901 (2014).

[4] Triana, B., Cha, J., Shademan, A., Krieger, A., Kang, J. U., and Kim, P. C., "Multispectral tissue analysis and classification towards enabling automated robotic surgery," in [*Proc. SPIE 8935, Advanced Biomedical and Clinical Diagnostic Systems XII*], 893527–893527, International Society for Optics and Photonics (2014).

[5] Delporte, C., Sautrot, S., Chouikha, M. B., Viénot, F., and Alquié, G., "Biological tissue identification using a multispectral imaging system," in [*Proc. SPIE 8659, Sensors, Cameras, and Systems for Industrial and Scientific Applications XIV*], 86590H–86590H, International Society for Optics and Photonics (2013).

[6] Khelifi, R., Adel, M., and Bourennane, S., "Multispectral texture characterization: application to computer aided diagnosis on prostatic tissue images," *EURASIP Journal on Advances in Signal Processing* **2012**, 1–13 (May 2012).

[7] Lu, G., Halig, L., Wang, D., Qin, X., Chen, Z. G., and Fei, B., "Spectral-spatial classification for noninvasive cancer detection using hyperspectral imaging," *Journal of biomedical optics* **19**(10), 106004–106004 (2014).

[8] Wirkert, S. J., Clancy, N. T., Stoyanov, D., Arya, S., Hanna, G. B., Schlemmer, H.-P., Sauer, P., Elson, D. S., and Maier-Hein, L., "Endoscopic sheffield index for unsupervised in vivo spectral band selection," in [*Computer-Assisted and Robotic Endoscopy*], 110–120, Springer (2014).

[9] Chambolle, A., "An algorithm for total variation minimization and applications," *Journal of Mathematical imaging and vision* **20**(1-2), 89–97 (2004).

[10] Hidović-Rowe, D. and Claridge, E., "Modelling and validation of spectral reflectance for the colon," *Physics in medicine and biology* **50**(6), 1071 (2005).

[11] Tou, J. Y., Tay, Y. H., and Lau, P. Y., "Recent trends in texture classification: a review," in [*Symposium on Progress in Information & Communication Technology*], **3**(2), 56–59 (2009).

[12] Ojala, T., Pietikäinen, M., and Mäenpää, T., "Multiresolution gray-scale and rotation invariant texture classification with local binary patterns," *IEEE Transactions on Pattern Analysis and Machine Intelligence* **24**(7), 971–987 (2002).

[13] Ahonen, T., Hadid, A., and Pietikainen, M., "Face description with local binary patterns: Application to face recognition," *IEEE Transactions on Pattern Analysis and Machine Intelligence* **28**(12), 2037–2041 (2006).

[14] Zhang, W., Shan, S., Gao, W., Chen, X., and Zhang, H., "Local gabor binary pattern histogram sequence (lgbphs): A novel non-statistical model for face representation and recognition," in [*Tenth IEEE International Conference on Computer Vision, 2005. ICCV 2005.*], **1**, 786–791, IEEE (2005).

[15] Lahdenoja, O., Poikonen, J., and Laiho, M., "Towards understanding the formation of uniform local binary patterns," *ISRN Machine Vision* **2013** (2013).

[16] Burges, C. J., "A tutorial on support vector machines for pattern recognition," *Data mining and knowledge discovery* **2**(2), 121–167 (1998).

[17] Scholkopf, B. and Smola, A. J., [*Learning with kernels: support vector machines, regularization, optimization, and beyond*], MIT press (2001).

[18] Maier-Hein, L., Groch, A., Bartoli, A., Bodenstedt, S., Boissonnat, G., Chang, P.-L., Clancy, N., Elson, D., Haase, S., Heim, E., et al., "Comparative validation of single-shot optical techniques for laparoscopic 3-d surface reconstruction," *IEEE Transactions on Medical Imaging* **33**(10), 1913–1930 (2014).

[19] Nolden, M., Zelzer, S., Seitel, A., Wald, D., Müller, M., Franz, A. M., Maleike, D., Fangerau, M., Baumhauer, M., Maier-Hein, L., et al., "The medical imaging interaction toolkit: challenges and advances," *International journal of computer assisted radiology and surgery* **8**(4), 607–620 (2013).

[20] Randen, T. and Husoy, J. H., "Filtering for texture classification: A comparative study," *IEEE Transactions on Pattern Analysis and Machine Intelligence* **21**(4), 291–310 (1999).

[21] Gadkari, D., "Image quality analysis using glcm," (2004).

[22] Crum, W. R., Hartkens, T., and Hill, D., "Non-rigid image registration: theory and practice," *The British Journal of Radiology* (2014).

[23] Wirkert, S. J., Kenngott, H., Mayer, B., Mietkowski, P., Wagner, M., Sauer, P., Clancy, N. T., Elson, D. S., and Maier-Hein, L., "Robust near real-time estimation of physiological parameters from megapixel multispectral images with inverse monte carlo and random forest regression," in [*Information Processing in Computer-Assisted Interventions (accepted)*], (2016).